

Determining parameters of Kerr-Newman black holes by shadow observation from finite distance and spatial infinity

Kenta Hioki^{1,*} and Umpei Miyamoto^{2,†}

¹*Sumitomo Mitsui Financial Group, Inc., 1-2,*

Marunouchi 1-chome, Chiyoda-ku, Tokyo 100-0005, Japan^a

²*Research and Education Center for Comprehensive Science,*

Akita Prefectural University, Akita 015-0055, Japan

Abstract

We present a method for determining the physical parameters of a Kerr-Newman black hole through shadow observation. In a system comprising a Kerr-Newman black hole, an observer, and a light source, the relevant parameters are mass M , specific angular momentum a , electric charge Q , inclination angle i , and distance r_o . We consider the cases where the observer is at either a finite distance or spatial infinity. Using our method, the dimensionless parameters $(a/M, Q/M, i)$ can be determined by observing the shadow contour of the Kerr-Newman black hole from spatial infinity. We analytically prove that the shadow contour of the Kerr-Newman black hole observed from spatial infinity is unique, where uniqueness is defined as the absence of two congruent shadow contours for distinct sets of dimensionless parameter values. This method is versatile and can be applied to a range of black hole solutions with charge. Additionally, we show analytically that the shadow contour of a Kerr-Newman black hole observed from a finite distance r_o is not unique, meaning that the parameters of a Kerr-Newman black hole at finite distance cannot be determined from shadow observations. This result reveals a new challenge and provides a clear direction for further research on black hole shadows.

^a The statements expressed in this paper are those of the authors and do not represent the views of Sumitomo

Mitsui Financial Group, Inc. or its staff.

* kenta.hioki@gmail.com

† umpei@akita-pu.ac.jp

CONTENTS

I. Introduction	2
II. Setup	5
A. Null geodesics	5
B. Light source and observer	7
C. Celestial coordinates and screen coordinates	8
D. Classes of null geodesics	9
E. Shadow of the black hole	11
III. Properties of shadows	12
A. Examples of apparent shapes	12
B. Non-uniqueness of apparent shape of the black hole at finite distance	12
IV. Parameter determination by analysis of apparent shape	18
A. Screen coordinates and Bardeen coordinates	18
B. Uniqueness of apparent shape on the Bardeen coordinates	19
C. Map from parameter space to apparent-shape library	21
D. Observables of apparent shape	22
E. Parameter determination	25
F. Demonstration	27
V. Conclusion	28
Acknowledgements	30
References	30

I. INTRODUCTION

A black hole is a fascinating celestial object that serves as the ultimate testing ground for studying the physics of strong gravitational fields. Observing a black hole shadow has long been a significant goal in physics. This shadow is formed when light emitted by matter surrounding the black hole is bent by the black hole's intense gravitational pull.

Recently, Earth-sized very long baseline interferometers achieved a milestone by capturing images of two black hole candidates. The first image captured M87* [1–7], and the second focused on Sgr A* [8–13]. Both images displayed a prominent ring, marking a major advancement in black hole imaging techniques. However, the darker central region, known as the shadow, has yet to be clearly identified. Further enhancements in observation equipment are needed to resolve these shadows with greater precision [4].

Some researchers suggest that the study of black hole imaging began with the derivation of the shadow contour, which is now known as the apparent shape. The apparent shape of a Schwarzschild black hole was first derived in Ref. [14], followed by that of a Kerr black hole in Ref. [15]. These foundational studies established the basis of shadow theory. Although these calculations focused on the apparent shapes of simple bare black holes without considering surrounding accretion disks, they highlighted the essential role of the photon sphere. This feature remains significant even in the shadow of a black hole with an accretion disk.

Many researchers have explored black hole shadows and methods for extracting physical information, such as a specific angular momentum of a black hole, through shadow observations [17–26]. In this paper, however, we emphasize that there is still potential to improve the accuracy of measuring black hole parameters via shadow analysis. In particular, further study is needed to determine whether information like a specific angular momentum and electric charge of a black hole can be obtained solely from shadow observations.

One way to investigate this possibility is examining whether the map from a parameter space to an image library is injective [27, 28]. It has been shown that the map from the parameter space to the apparent-shape library for a bare Kerr black hole is indeed injective [27, 29]. Here, the apparent-shape library refers to the set of all possible apparent shapes that can be produced within the framework of the given gravitational theory and model. The result suggests that the dimensionless specific angular momentum and inclination angle of a Kerr black hole can be uniquely determined by observing its apparent shape.

Determining (1) whether an object is indeed a black hole, (2) identifying the specific black hole solution, and (3) accurately measuring its physical parameters based solely on shadow images is a challenging problem that requires extensive research. It is essential to generate a wide range of models for relativistic objects, thereby building an apparent-shape library that incorporates diverse parameters. Moreover, investigating the injectivity of the map is critical. If the map is not injective, it indicates the presence of images that correspond to

different models and parameter configurations, making it impossible to uniquely determine the model based on shadow observations alone. These research efforts are ongoing, and further studies are necessary.

As a first step toward addressing this problem, we assume that the black hole solution of the observed object has been identified, and it must be demonstrated that its parameters can be determined from shadow observations. When the target object is a black hole with three physical parameters (mass, angular momentum, and charge), no method has yet been proposed to uniquely determine these parameters from shadow observations alone, rather than merely constraining them.

For this purpose, we assume that the observed object is a Kerr-Newman black hole. The system comprising the Kerr-Newman black hole and the observer includes the physical quantities of mass M , specific angular momentum a , electric charge Q , inclination angle i , and distance r_o . We consider both cases in which the observer is at a finite distance and at spatial infinity.

For the first time in this paper, we show with a concrete method that the dimensionless parameters $(a/M, Q/M, i)$ can be uniquely determined by observing the shadow when the observer is at spatial infinity. The key point is that the aforementioned map from the parameter space to the image library is injective. This method can be applied to various black hole solutions with charge and is highly versatile.

We also show analytically that there is uniqueness in the contour of the black hole shadow when the observer is at spatial infinity. Uniqueness is defined as the absence of two congruent apparent shapes for two distinct dimensionless parameter values. The uniqueness of the apparent shape is the basis of our method for determining dimensionless parameters from shadow observations.

Surprisingly, we analytically prove that uniqueness does not hold for the shadow contour of the Kerr-Newman black hole when the distance r_o of the black hole is finite. This is a different feature from the case of the apparent shape of the Kerr black hole at finite distance [29]. This will be a problem to be solved in the future when there is an opportunity to observe black holes from a finite distance. It would be interesting to consider what would happen to this point if a more realistic model were considered, such as a black hole with an accretion disk.

The structure of this paper is as follows. In Sec. II, we begin the analysis by deriving the

null geodesic equations around the Kerr-Newman black hole and describing how to construct an apparent shape from these geodesics. In Sec. III, we present examples of the apparent shapes of the Kerr-Newman black hole at finite distances and then analytically demonstrate the non-uniqueness of these shapes. In Sec. IV, we analytically prove the uniqueness of the apparent shape in Bardeen coordinates. We also propose a method to systematically construct observables that characterize the apparent shape of Kerr-Newman black holes, showing that the dimensionless parameters of the system can be determined from shadow observations. In the final section, we summarize our analysis and discuss future prospects. We use geometrized units, where $c = G = 1$.

II. SETUP

A. Null geodesics

The Kerr-Newman spacetime is a stationary, axisymmetric, and asymptotically flat solution of the Einstein-Maxwell theory [30]. The Kerr-Newman metric in Boyer-Lindquist coordinates has the form

$$g_{\mu\nu}dx^\mu dx^\nu = - \left(1 - \frac{2Mr - Q^2}{\Sigma}\right) dt^2 + \frac{\Sigma}{\Delta} dr^2 + \Sigma d\theta^2 - \frac{(2Mr - Q^2) 2a \sin^2 \theta}{\Sigma} dt d\phi + \frac{A \sin^2 \theta}{\Sigma} d\phi^2, \quad (1)$$

where $x^\mu = (t, r, \theta, \phi)$ ($\mu, \nu = 0, 1, 2, 3$),

$$\begin{aligned} \Sigma(r, \theta) &:= r^2 + a^2 \cos^2 \theta, \\ \Delta(r) &:= r^2 - 2Mr + a^2 + Q^2, \\ A(r, \theta) &:= (r^2 + a^2)^2 - a^2 \Delta \sin^2 \theta. \end{aligned} \quad (2)$$

The parameters M , a , and Q are the mass, specific angular momentum, and electric charge of the spacetime, respectively. If $0 \leq a^2 + Q^2 \leq M^2$, then an event horizon exists in the spacetime, and the metric describes a black hole. The radii of the outer and inner horizons are denoted by r_+ and r_- , respectively. The Kerr-Newman metric contains Kerr ($a \neq Q = 0$), Reissner-Nordström ($a = 0 \neq Q$), and Schwarzschild ($a = Q = 0$) metrics as special cases.

We shall solve the null geodesic equation to find the trajectory $x^\mu(\lambda)$ of a massless test particle. We have four independent constants of motion in involution for geodesics in the Kerr-Newman black hole, making the geodesic equation completely integrable.

The Lagrangian of the massless test particle in the spacetime is expressed as:

$$\mathcal{L} = \frac{1}{2} g_{\mu\nu} \dot{x}^\mu \dot{x}^\nu, \quad (3)$$

$$\dot{x}^\mu := \frac{dx^\mu}{d\lambda}. \quad (4)$$

We derive the energy E and the axial component of the angular momentum L of the test particle:

$$E := -\frac{\partial \mathcal{L}}{\partial \dot{t}} = \left(1 - \frac{2Mr - Q^2}{\Sigma}\right) \dot{t} + \frac{(2Mr - Q^2) 2a \sin^2 \theta}{\Sigma} \dot{\phi} \quad (5)$$

and

$$L := \frac{\partial \mathcal{L}}{\partial \dot{\phi}} = -\frac{(2Mr - Q^2) 2a \sin^2 \theta}{\Sigma} \dot{t} + \frac{A \sin^2 \theta}{\Sigma} \dot{\phi}. \quad (6)$$

These quantities \mathcal{L} , E , and L , along with \mathcal{Q} (known as the Carter constant [31]), are conserved, highlighting their roles as constants of motion.

We denote the four-momentum of a massless test particle by k^μ , where

$$k^\mu = \frac{dx^\mu}{d\tilde{\lambda}}. \quad (7)$$

Here, $\tilde{\lambda}$, defined as $\tilde{\lambda} := \lambda E$, serves as the affine parameter. We introduce two conserved quantities for null geodesics ($\mathcal{L} = 0$): $\ell := L/E$ and $\mathbb{Q} := \mathcal{Q}/E^2$. Consequently, this leads us to obtain the following set of first-order differential equations:

$$\Sigma k^t = \frac{A - a\ell(2Mr - Q^2)}{\Delta}, \quad (8)$$

$$\Sigma k^r = \pm \sqrt{R}, \quad (9)$$

$$\Sigma k^\theta = \pm \sqrt{\Theta}, \quad (10)$$

$$\Sigma k^\phi = \frac{a(2Mr - Q^2) + \ell \csc^2 \theta (\Sigma - 2Mr + Q^2)}{\Delta}, \quad (11)$$

where

$$K := \mathbb{Q} + (a - \ell)^2, \quad (12)$$

$$R(r) := (r^2 + a^2 - a\ell)^2 - K\Delta, \quad (13)$$

$$\Theta(\theta) := K - (a \sin \theta - \ell \csc \theta)^2. \quad (14)$$

B. Light source and observer

If the initial conditions are set, the trajectory of the massless test particle can be found according to the geodesic equation.

We consider the setting of the light source. For astronomical black holes such as M87* to be the object of observation, let us assume that the black hole has neither an accretion flow nor an accretion disc surrounding it [32, 33]. This means that we assume that the Kerr-Newman black hole is bare. In the next paragraphs, we will explain our assumptions about the observer in more detail, where we assume that the distance between the black hole and the observer takes a finite value r_o . Then, we assume that a sphere of radius $r = r_e = \text{const.}$, where $r_o < r_e$, is the light source and that each point on it uniformly emits a null ray [34].

Next, let us clarify the setting of the observer receiving the null ray. Possible candidates include zero-angular-momentum observers [15] and Carter's observers [34], each of which exhibits distinct azimuthal motions [35]. Our aim is to demonstrate the existence of an observer capable of determining the black hole parameters. Selecting either observer type is sufficient for this purpose. In this paper, we choose Carter's observer.

We introduce a tetrad of basis vectors,

$$e_{(t)} := \frac{(r^2 + a^2) \partial_t + a \partial_\phi}{\sqrt{\Sigma \Delta}}, \quad (15)$$

$$e_{(r)} := -\sqrt{\frac{\Delta}{\Sigma}} \partial_r, \quad (16)$$

$$e_{(\theta)} := \frac{1}{\sqrt{\Sigma}} \partial_\theta, \quad (17)$$

$$e_{(\phi)} := -\frac{a \sin \theta \partial_t + \csc \theta \partial_\phi}{\sqrt{\Sigma}}. \quad (18)$$

The timelike vector $e_{(t)}|_{(r,\theta)=(r_o,i)}$ can be interpreted as the four-velocity of the observer and the vector $e_{(r)}|_{(r,\theta)=(r_o,i)}$ gives the spatial direction towards the black hole [see Fig. 1(a)]. Since Eqs. (10) and (11) are defined on $\theta \in (0, \pi)$, we assume $i \in (0, \pi/2)$.

We assume that the observer is at finite distance r_o from the black hole. While the observer could be located anywhere within the domain of outer communication, we limit this range to $r_o \in [5M, \infty]$. This restriction is adequate for demonstrating that the black hole's parameters can be determined.

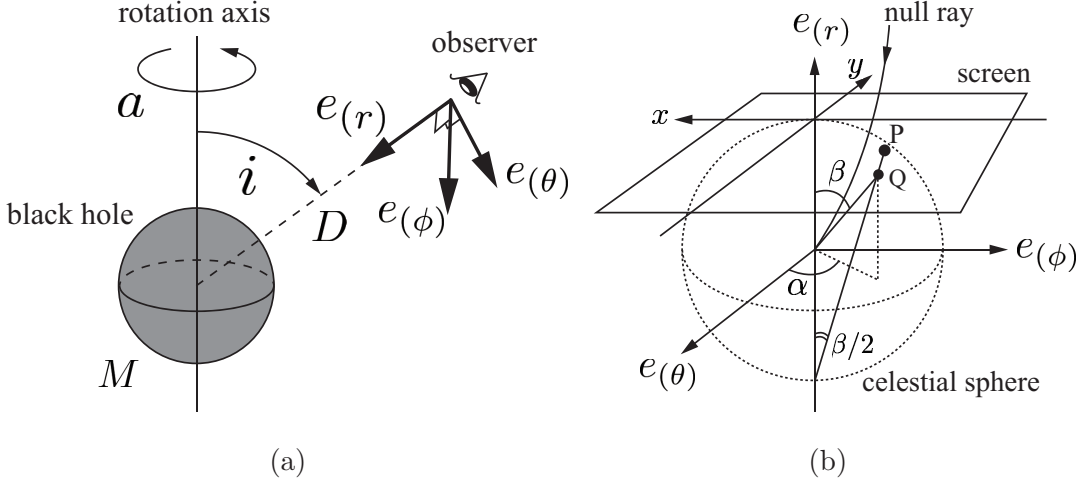


FIG. 1. (a) A schematic picture showing a unit sphere in which the center coincides with that of the Kerr-Newman black hole. The observer is located at $(r, \theta) = (r_o, i)$. (b) A schematic picture showing a unit celestial sphere for the observer. The direction of $e(r)$ is a direction to the Kerr-Newman black hole from the observer. (α, β) is a celestial coordinate system, which is used to specify the incident angle of the null ray into the observer. Q is the point where the tangent of null ray at the center of the celestial sphere crosses the unit sphere. P is the two-dimensional image made by the null ray.

C. Celestial coordinates and screen coordinates

In the remaining subsections of Sec. II, we formulate how the apparent shape, which is the contour of the shadow, is formed by null rays. Specifically, we present the map from the parameters to the apparent shape.

The tangent vector of the null geodesic $x^\mu(\tilde{\lambda})$ can be written, using four-momentum k^μ , as follows:

$$\frac{d}{d\tilde{\lambda}} = k^\mu \partial_\mu. \quad (19)$$

As can be seen from Fig. 1(b), this tangent vector at the observer can be expressed using the two incident angles (α, β) of the null geodesic to the observer as follows:

$$\left. \frac{d}{d\tilde{\lambda}} \right|_{(r,\theta)=(r_o,i)} = \epsilon \left(-e_{(t)} + \cos \beta e_{(r)} + \sin \beta \cos \alpha e_{(\theta)} + \sin \beta \sin \alpha e_{(\phi)} \right), \quad (20)$$

where ϵ is a scalar factor. We refer to these two incident angles (α, β) as the celestial coordinates of the observer. The scale factor ϵ can be derived from the orthogonality of the

basis vectors:

$$\epsilon = - \frac{r^2 + a^2 - a\ell}{\sqrt{\Sigma\Delta}} \Big|_{(r,\theta)=(r_o,i)}. \quad (21)$$

Using Eqs. (19), (20), and (21), we write down the equations relating the celestial coordinates, constants of motion and parameters.

$$\sin \alpha = \frac{\sin \theta}{\sqrt{\Delta} \sin \beta} \left(\frac{\Delta \Sigma k^\phi}{r^2 + a^2 - a\ell} - a \right) \Big|_{(r,\theta)=(r_o,i)}, \quad (22)$$

$$\cos \beta = \frac{\Sigma k^r}{r^2 + a^2 - a\ell} \Big|_{(r,\theta)=(r_o,i)}. \quad (23)$$

Let us define the screen coordinates (x, y) in which the apparent shape of the black hole is depicted, as shown in Fig. 1(b) [34]. The celestial coordinates are transformed to the screen coordinates as follows:

$$x = -2 \sin \alpha \tan \frac{\beta}{2}, \quad (24)$$

$$y = -2 \cos \alpha \tan \frac{\beta}{2}. \quad (25)$$

A circle with center at the origin and radius 2 in the screen coordinates (x, y) corresponds to the celestial equator.

D. Classes of null geodesics

We consider two important classes of null geodesics forming the apparent shape. The first is the class of spherical photon orbits, and the second is the class of principal null geodesics.

Whether a null geodesic emitted from a light source has a turning point after heading toward a black hole and reaches the observer depends on the conserved quantities of the null geodesic. The critical value of the conserved quantities that determines this is the value of the conserved quantities of the null geodesic that winds around the spherical photon orbit an infinite number of times. We can say that the value of the conserved quantities of the spherical photon orbits is critical. This is because spherical photon orbits and the null geodesics that wind around those orbits are null geodesics with different initial conditions, but with the same conserved quantity values.

A null geodesic with constant radial motion is called a *spherical photon orbit*. The radius r_s of a spherical photon orbit is obtained by

$$R(r_s) = 0, \quad R'(r_s) = 0. \quad (26)$$

For a spherical photon orbit of radius r_s to exist, there is an additional condition that θ must satisfy the following inequality

$$\Theta(\theta) \geq 0. \quad (27)$$

The conserved quantities ℓ and \mathbb{Q} satisfying Eq. (26) are denoted by ℓ_s and \mathbb{Q}_s , where

$$\ell_s = \frac{r_s^2 + a^2}{a} - \frac{2r_s\Delta(r_s)}{a(r_s - M)}, \quad (28)$$

$$\mathbb{Q}_s = -\frac{r_s^2 [r_s^2 (r_s - 3M)^2 - 4Mr_s (a^2 + Q^2) + 4Q^2\Delta]}{a^2(r_s - M)^2}, \quad (29)$$

respectively. These quantities ℓ_s and \mathbb{Q}_s are conserved quantities for spherical photon orbits of radius r_s . Considering the position of the observer, it can be seen from Eqs. (27), (28), and (29) that the radius r_s must satisfy $\Theta(i)|_{(\ell, \mathbb{Q})=(\ell_s, \mathbb{Q}_s)} \geq 0$.

Substituting Eqs. (28) and (29) into Eq. (12), we find that the conserved quantity K of the spherical photon orbits is

$$K = K_s := \frac{4r_s^2\Delta(r_s)}{(r_s - M)^2}. \quad (30)$$

Since the conserved quantity K is generally non-negative [31], the radius r_s of a spherical photon orbit must lie within the range

$$r_s \in (-\infty, r_-] \cup [r_+, \infty). \quad (31)$$

This is a necessary condition for the existence of spherical photon orbits of radius r_s .

The condition under which the spherical photon orbit is unstable in the radial direction is

$$R''(r_s) > 0. \quad (32)$$

This inequality is equivalent to

$$r_s \in (-\infty, 0) \cup (r_u, \infty), \quad (33)$$

where $r_u := M - [M(M^2 - a^2 - Q^2)]^{1/3}$.

As can be seen from the conditions (31) and (33), if an unstable spherical photon orbit exists, its radius r_s satisfies the following:

$$r_s \in (-\infty, 0) \cup [r_+, \infty). \quad (34)$$

Thus, all spherical photon orbits outside the event horizon that are important for the apparent shape are unstable in the radial direction. For the sake of later discussion, we define I as the set of radii of the existing unstable spherical photon orbits.

Another important class is that of *principal null geodesics*. The principal null geodesics reach the observer straight ($\theta = \text{const.}$) from the black hole, without any turning points in the radial direction.

The principal null geodesic is the null geodesic for which the conserved quantity K is $K = 0$. When we assume that the principal null geodesic reaches the observer, Eq. (10) implies that $\theta = i$. These give us two conserved quantities ℓ_p and \mathbb{Q}_p of the principal null geodesic:

$$\ell_p = a \sin^2 i, \quad (35)$$

$$\mathbb{Q}_p = -a^2 \cos^4 i. \quad (36)$$

The origin of the screen coordinates defined in Fig. 1 is related to the conserved quantity ℓ_p of the principal null geodesics. This point will be discussed in more detail in Sec. IV.

E. Shadow of the black hole

We describe how the apparent shape, the shadow contour of a black hole, can be drawn. To do so, we describe the role of the unstable spherical photon orbits and the principal null geodesics in the casting of the shadow.

To consider unstable spherical photon orbits, let us trace the geodesics reaching the observer back to their starting points. Null geodesics that do not start from a light source are null geodesics forming the shadow of a black hole. Such geodesics can be classified into two categories. One is a null geodesic whose starting point is a black hole. The other is a null geodesic that is winding around a spherical photon orbit an infinite number of times.

We shall draw a curve c in screen coordinates corresponding to a geodesic winding around a spherical photon orbit an infinite number of times. The functions $x(\ell_s, q_s)$ and $y(\ell_s, \mathbb{Q}_s)$ can be obtained by substituting Eqs. (9), (11), (22), and (23) into Eqs. (24) and (25). Then, using Eqs. (28) and (29), the functions become $x(r_s)$ and $y(r_s)$. We can draw a closed curve c in the screen coordinates for fixed values of (M, r_o, a, Q, i) by varying r_s over the entire range of I .

The closed curve c is the boundary between the dim and bright areas on the screen coordinates [16, 17, 27]. Intuitively, the inside of the closed curve is considered to be the dark area, but let us briefly explain this using the principal null geodesic. Since the principal null geodesic reaches the observer from the black hole, it is the point that constitutes the dim part on the screen coordinates. Since this point is located inside the closed curve, the interior of the closed curve is the dim part, the shadow [27]. Of course, the closed curve itself also constitutes part of the shadow. Thus, the closed curve c is the apparent shape of the black hole.

III. PROPERTIES OF SHADOWS

A. Examples of apparent shapes

In Figs. 2 and 3, we present the apparent shapes of the Kerr-Newman black holes for four values of dimensionless spin parameter $a/M = 0.4, 0.6, 0.8,$ and 0.999 , four values of dimensionless electric charge $Q/M = 0.04, 0.5999, 0.7999,$ and 0.9165 , three values of dimensionless distance $r_o/M = 10, 30,$ and 50 , and two values of inclination angle $i = 90^\circ$ and 60° . It can be seen from Figs 2 and 3. that the deformation of the apparent shape depends mainly on a/M and Q/M , i , and that the size depends mainly on r_o/M . We will see in Sec. IV that the parameter r_o/M also deform the apparent shape. Note that the apparent shapes with different r_o/M but the same values of other parameters are *not similar*. Namely, we mean that one shape cannot be obtained from the other by uniform scaling, possibly with translation, rotation, or reflection.

B. Non-uniqueness of apparent shape of the black hole at finite distance

To find out the characteristics of the apparent shape, we need to analyze the corresponding curves on the celestial coordinates (α, β) . As can be seen from Eqs. (22) and (23), the functions $\sin \alpha$ and $\cos \beta$ are not explicitly dependent on M . We introduce dimensionless parameters:

$$r_{o*} := \frac{r_o}{M}, \quad a_* := \frac{a}{M}, \quad Q_* := \frac{Q}{M}, \quad r_* := \frac{r_s}{M}. \quad (37)$$

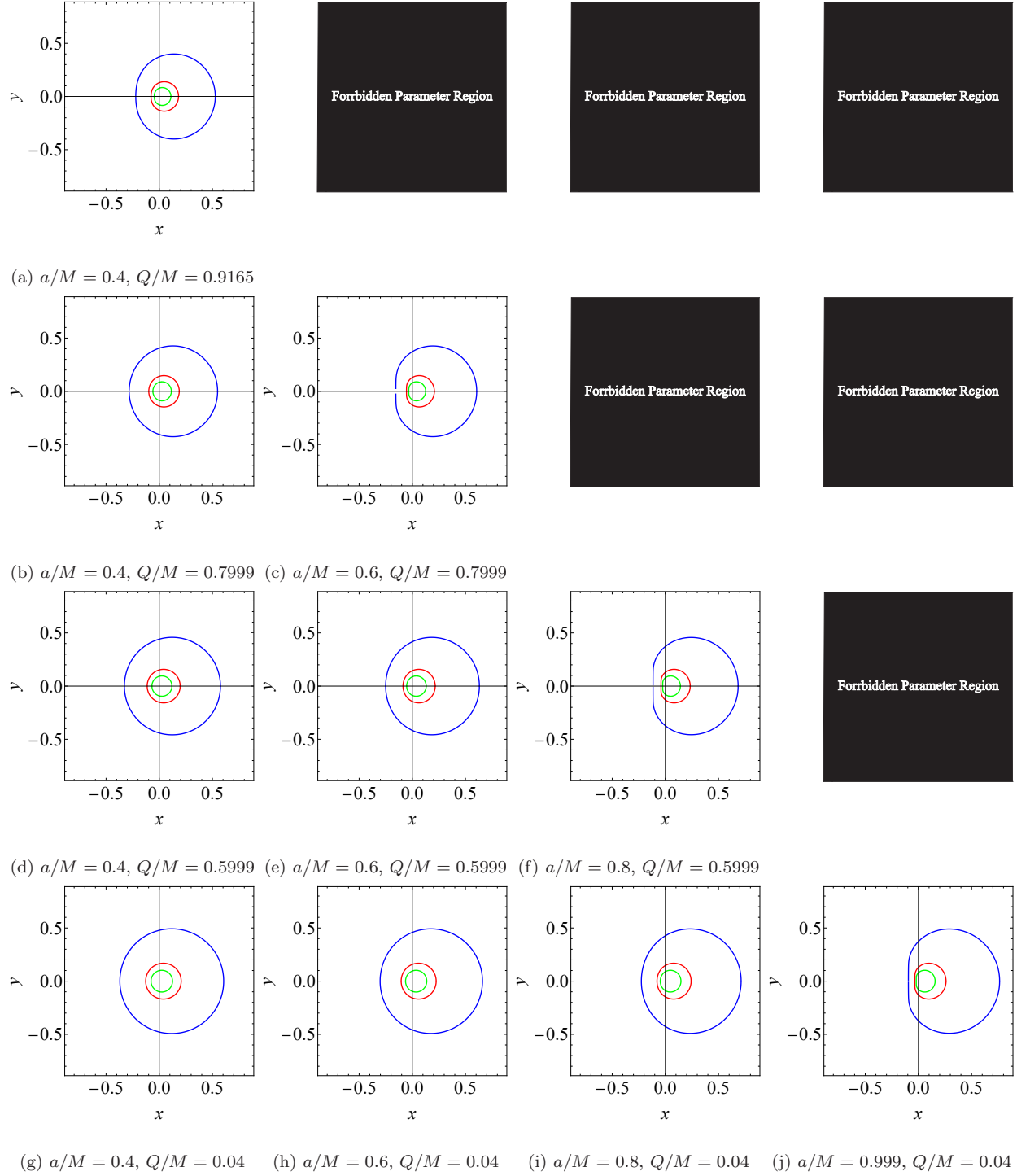


FIG. 2. Shadows of the Kerr-Newman black holes with the inclination angle $i = 90^\circ$. The blue, red, and green curves are the apparent shape of the black hole at dimensionless distances r_o/M of 10, 30, and 50, respectively.

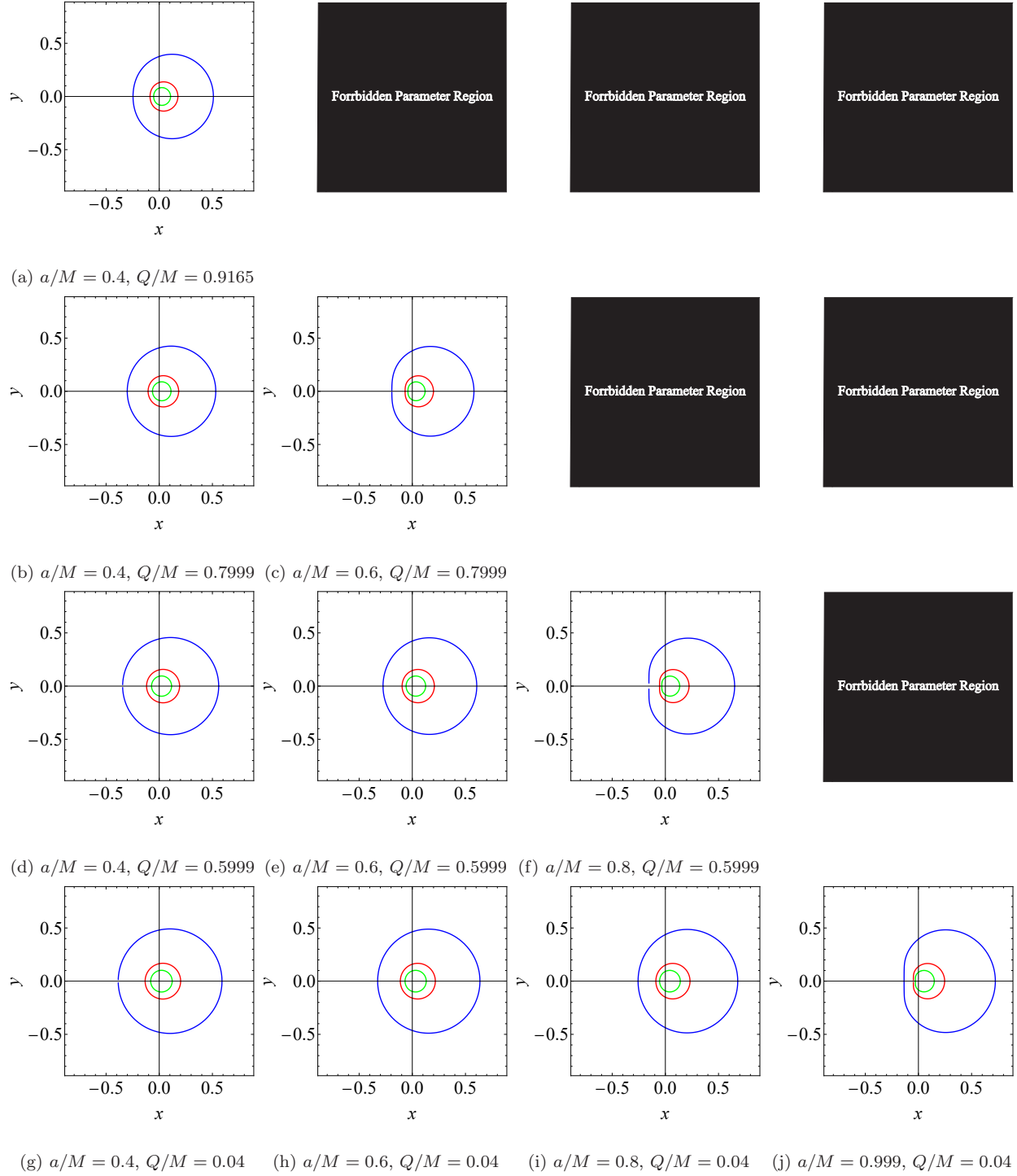


FIG. 3. Shadows of the Kerr-Newman black holes with the inclination angle $i = 60^\circ$. The blue, red, and green curves are the apparent shape of the black hole at dimensionless distances r_o/M of 10, 30, and 50, respectively.

We prove the non-uniqueness of the apparent shape on the screen coordinates of the Kerr-Newman black hole. We refer to uniqueness as the absence of two congruent apparent shapes at the same position on the screen coordinates for two values of parameters (r_{o*}, a_*, Q_*, i) .

The function $\sin^2 \alpha$ is a rational function with r_* as a variable. Note that this function is defined at $a_* \neq 0$. In general, a necessary and sufficient condition for two polynomials to have a common factor is that the resultant of the two polynomials is zero [36]. Let us derive the condition under which the numerator and denominator of the rational function $\sin^2 \alpha$ has a common factor:

$$\text{Res}(p(r_*), q(r_*), r_*) = 0, \quad (38)$$

where $p(r_*)$ and $q(r_*)$ are the numerator and denominator of $\sin^2 \alpha$, respectively. Since the resultant of the two polynomials is equivalent to the determinant of the Sylvester matrix of the two polynomials, the condition follows:

$$\begin{aligned} & a_*^{20} \sin^{12} i \cot^8 i (a_*^2 + Q_*^2 - 1)^2 [3a_*^4 + 8Q_*^4 \\ & + 8a_*^2 (2 + Q_*^2) + 4a_*^2 (4 - a_*^2 - 2Q_*^2) \cos 2i + a_*^4 \cos 4i]^2 = 0. \end{aligned} \quad (39)$$

Looking carefully at Eq. (39), we find that the condition can be simplified:

$$a_*^2 + Q_*^2 = 1 \quad \text{or} \quad i = \frac{\pi}{2}. \quad (40)$$

This implies that the extremality of the black hole is related to the reducibility of $\sin^2 \alpha$.

From the condition, the rational function $\sin^2 \alpha$ is found to be irreducible in each of the four cases.

$$\sin^2 \alpha = \begin{cases} \frac{\sum_{n=0}^6 a_n r_*^n}{\sum_{n=0}^4 b_n r_*^n} & (0 < a_*^2 + Q_*^2 < 1 \text{ and } i \neq \pi/2) \\ \frac{\sum_{n=0}^4 \hat{a}_n r_*^n}{\sum_{n=0}^2 \hat{b}_n r_*^n} & (0 < a_*^2 + Q_*^2 < 1 \text{ and } i = \pi/2) \\ \frac{\sum_{n=0}^4 \bar{a}_n r_*^n}{\sum_{n=0}^2 \bar{b}_n r_*^n} & (a_*^2 + Q_*^2 = 1 \text{ and } i \neq \pi/2) \\ \frac{\sum_{n=0}^2 \tilde{a}_n r_*^n}{b_0} & (a_*^2 + Q_*^2 = 1 \text{ and } i = \pi/2) \end{cases}, \quad (41)$$

where

$$\begin{aligned} a_0 &= 4a_*^4 \cos^4 i, & a_1 &= -4a_*^2 \cos^2 i (a_*^2 \cos 2i - 3a_*^2 - 4Q_*^2), \\ a_2 &= 9a_*^4 + 16Q_*^4 + 12a_*^2 (-1 + 2Q_*^2) - 2a_*^2 (6 + 3a_*^2 + 4Q_*^2) \cos 2i + a_*^4 \cos^2 2i, \\ a_3 &= 16 (-2a_*^2 - 3Q_*^2 + a_*^2 \cos 2i), & a_4 &= 4 (9 + 3a_*^2 + 4Q_*^2 - a_*^2 \cos 2i), \\ a_5 &= -24, & a_6 &= 4, \\ b_0 &= 0, & b_1 &= 0, & b_2 &= 16a_*^2 (a_*^2 + Q_*^2) \sin^2 i, & b_3 &= -32a_*^2 \sin^2 i, & b_4 &= 16a_*^2 \sin^2 i, \end{aligned}$$

$$\hat{a}_0 = 4(a_*^2 + Q_*^2)^2, \quad \hat{a}_1 = -12(a_*^2 + Q_*^2), \quad \hat{a}_2 = 9 + 4a_*^2 + 4Q_*^2, \quad \hat{a}_3 = -6, \quad \hat{a}_4 = 1,$$

$$\hat{b}_0 = 4a_*^2(a_*^2 + Q_*^2), \quad \hat{b}_1 = -8a_*^2, \quad \hat{b}_2 = 4a_*^2,$$

$$\bar{a}_0 = 4a_*^4 \cos^4 i, \quad \bar{a}_1 = 16a_*^2 \cos^2 i, \quad \bar{a}_2 = 4(4 - a_*^2 - a_*^2 \cos 2i), \quad \bar{a}_3 = -16, \quad \bar{a}_4 = 4,$$

$$\bar{b}_0 = 0, \quad \bar{b}_1 = 0, \quad \bar{b}_2 = 16a_*^2 \sin^2 i,$$

and

$$\tilde{a}_0 = 4, \quad \tilde{a}_1 = -4, \quad \tilde{a}_2 = 1,$$

$$\tilde{b}_0 = 4a_*^2.$$

We find that $\cos^2 \beta$ is also a rational function of r_* . As before, let us check the condition under which the numerator and denominator of this rational function $\cos^2 \beta$ has a common factor:

$$\text{Res}(l(r_*), m(r_*), r_*) = 0, \quad (42)$$

where $l(r_*)$ and $m(r_*)$ are the numerator and denominator of $\cos^2 \beta$, respectively. We compute the determinant of the Sylvester matrix of polynomials, $l(r_*)$ and $m(r_*)$, and write down the condition:

$$r_{o*}^8 (a_*^2 + Q_*^2 - 1)^2 [a_*^2 + Q_*^2 + (r_{o*} - 2)r_{o*}]^8 [a_*^2 + Q_*^2 + (r_{o*} + 2)r_{o*}]^2 = 0. \quad (43)$$

We see that the condition for the function $\cos^2 \beta$ to be reducible is the condition for the black hole to be extreme:

$$a_*^2 + Q_*^2 = 1. \quad (44)$$

Thus, if we divide the case into two cases, a nonextreme black hole and an extreme black hole, the function $\cos^2 \beta$ is irreducible as follows:

$$\cos^2 \beta = \begin{cases} \frac{\sum_{n=0}^6 e_n r_*^n}{\sum_{n=0}^6 g_n r_*^n} & (0 \leq a_*^2 + Q_*^2 < 1) \\ \frac{\sum_{n=0}^4 \bar{e}_n r_*^n}{\sum_{n=0}^4 \bar{g}_n r_*^n} & (a_*^2 + Q_*^2 = 1) \end{cases}, \quad (45)$$

where

$$e_0 = r_{o*}^4, \quad e_1 = -2[2(a_*^2 + Q_*^2)r_{o*}^2 + r_{o*}^4], \quad e_2 = r_{o*}[8(a_*^2 + Q_*^2) + 6r_{o*} + r_{o*}^3],$$

$$e_3 = -4[(a_*^2 + Q_*^2) + 4r_{o*}], \quad e_4 = 9 - 2r_{o*}(r_{o*} - 4), \quad e_5 = -6, \quad e_6 = 1,$$

$$g_0 = r_{o*}^4, \quad g_1 = -2[2(a_*^2 + Q_*^2)r_{o*}^2 + r_{o*}^4], \quad g_2 = 6r_{o*}^2 + [2(a_*^2 + Q_*^2) + r_{o*}^2]^2,$$

$$g_3 = -4[3(a_*^2 + Q_*^2) + 2r_{o*}^2], \quad g_4 = 9 + 4(a_*^2 + Q_*^2) + 2r_{o*}^2, \quad g_5 = -6, \quad g_6 = 1,$$

and

$$\begin{aligned}\bar{e}_0 &= r_{o*}^4, & \bar{e}_1 &= -4r_{o*}^2, & \bar{e}_2 &= -2r_{o*}^2 + 8r_{o*}, & \bar{e}_3 &= -4, & \bar{e}_4 &= 1, \\ \bar{g}_0 &= r_{o*}^4, & \bar{g}_1 &= -4r_{o*}^2, & \bar{g}_2 &= 4 + 2r_{o*}^2, & \bar{g}_3 &= -4, & \bar{g}_4 &= 1.\end{aligned}$$

Let us consider the case where $a_* \neq 0$.

For a nonextreme Kerr-Newman black hole viewed from outside the edge-on perspective ($i \neq \pi/2$), we assume that $\sin^2 \alpha(r_*; a_*, Q_*, i) = \sin^2 \alpha(r_*; a'_*, Q'_*, i')$. From the coefficients b_2 and b_4 , we derive $a_*^2 \sin^2 i = a'^2_* \sin^2 i'$ and $a_*^2 + Q_*^2 = a'^2_* + Q'^2_*$. Analyzing the coefficient a_3 , we conclude that $a_* = a'_*$, $Q_* = Q'_*$, and $i = i'$. Additionally, we assume that $\cos^2 \beta(r_*; r_{o*}, a_*, Q_*) = \cos^2 \beta(r_*; r'_{o*}, a'_*, Q'_*)$. From the coefficient e_0 , we deduce that $r_{o*} = r'_{o*}$.

In the case of a nonextreme Kerr-Newman black hole viewed edge-on ($i = \pi/2$), we assume that $\sin^2 \alpha(r_*; a_*, Q_*, \pi/2) = \sin^2 \alpha(r_*; a'_*, Q'_*, \pi/2)$. From the coefficients \hat{a}_1 and \hat{b}_2 , we determine that $a_* = a'_*$ and $Q_* = Q'_*$. We also assume that $\cos^2 \beta(r_*; r_{o*}, a_*, Q_*) = \cos^2 \beta(r_*; r'_{o*}, a'_*, Q'_*)$. By comparing e_0 , we establish that $r_{o*} = r'_{o*}$.

Considering the case of an extreme Kerr-Newman black hole viewed from outside the edge-on perspective ($i \neq \pi/2$), we assume that $\sin^2 \alpha(r_*; a_*, Q_*, i) = \sin^2 \alpha(r_*; a'_*, Q'_*, i')$. From the coefficients \bar{a}_1 and \bar{b}_2 , we determine that $a = a'$ and $i = i'$, assuming an extreme black hole, thus $Q = Q'$. We further assume that $\cos^2 \beta(r_*; r_{o*}, a_*, Q_*) = \cos^2 \beta(r_*; r'_{o*}, a'_*, Q'_*)$. By comparing \bar{e}_0 , we establish that $r_{o*} = r'_{o*}$.

In the case of an extreme Kerr-Newman black hole viewed edge-on ($i = \pi/2$), we assume that $\sin^2 \alpha(r_*; a_*, Q_*, \pi/2) = \sin^2 \alpha(r_*; a'_*, Q'_*, \pi/2)$. By comparing \tilde{b}_0 , we establish that $a_* = a'_*$. The assumption leads us to conclude that $Q_* = Q'_*$. Further assuming that $\cos^2 \beta(r_*; r_{o*}, a_*, Q_*) = \cos^2 \beta(r_*; r'_{o*}, a'_*, Q'_*)$, we verify that $r_{o*} = r'_{o*}$ by comparing \bar{e}_0 .

Now, let us consider the case where $a_* = 0$. We examine the apparent shape of the Reissner-Nordström black hole. Since the Reissner-Nordström black hole is spherically symmetric, it has no rotation axis, and therefore the parameter i is not relevant.

The apparent shape of the Reissner-Nordström black hole is a circle. As you can see from Eqs. (24) and (25), the square of radius of the apparent shape is $4 \tan^2 \beta/2$.

The function $\tan^2 \beta/2$ is a monotonically decreasing function of $\cos \beta$. Note that there is a relation: $\tan^2 \beta/2 = (1 - \cos \beta) / (1 + \cos \beta)$. Since $\cos \beta$ is positive, the value of $\cos^2 \beta$ is uniquely determined for the value of $\tan^2 \beta/2$.

The radius r_* of the unstable spherical photon orbit of the Reissner-Nordström black hole is a monotonically decreasing function of the parameter Q_* [31]:

$$r_*(Q_*) = \frac{3}{2} \left[1 + \left(1 - \frac{8}{9} Q_*^2 \right)^{1/2} \right]. \quad (46)$$

We derive that there are an infinite number of tuples of (r_{o*}, Q_*) for which $\cos^2 \beta$ has the same value \mathcal{C} :

$$\cos^2 \beta(r_*(Q_*); r_{o*}, 0, Q_*) = \mathcal{C} = \text{const}. \quad (47)$$

Using Eq. (46), Eq. (47) can be written explicitly as follows:

$$\begin{aligned} & \left[1 + \left(1 - \frac{8}{9} Q_*^2 \right)^{1/2} - \frac{2}{3} r_{o*} \right]^2 \left(\frac{8}{3} Q_*^4 + r_{o*} \left\{ 8 \left[1 + \left(1 - \frac{8}{9} Q_*^2 \right)^{1/2} \right] \right. \right. \\ & \left. \left. + r_{o*} \left[\frac{5}{3} + \left(1 - \frac{8}{9} Q_*^2 \right)^{1/2} \right] \right\} - 4 Q_*^2 \left\{ 1 + \left(1 - \frac{8}{9} Q_*^2 \right)^{1/2} \right. \right. \\ & \left. \left. + r_{o*} \left[\frac{1}{3} r_{o*} + \frac{5}{3} + \left(1 - \frac{8}{9} Q_*^2 \right)^{1/2} \right] \right\} \right) = \frac{2\mathcal{C}}{9} r_{o*}^4 \left[\frac{1}{3} + \left(1 - \frac{8}{9} Q_*^2 \right)^{1/2} \right]^2. \quad (48) \end{aligned}$$

Equation (48) is a quadratic equation for r_{o*} , and by checking the coefficients, we can see that it has four real solutions. Then, for example, when $\mathcal{C} = 0.9$, we can find that there are infinite number of solutions (r_{o*}, Q_*) in the region $r_{o*} \geq 5$ for Eq. (48). The apparent shapes of the Reissner-Nordström black holes for such values of (r_{o*}, Q_*) are all congruent. This result can be understood that when $a_* = 0$, the value of the radius varies depending on the parameters r_{o*} and Q_* , but it is not possible to distinguish which parameter is causing the effect.

Thus, only when the specific angular momentum is non-zero, the apparent shape on the screen coordinates of the Kerr-Newman black hole is unique. Generally, uniqueness does not hold for the apparent shape of the Kerr-Newman black hole at finite distance.

IV. PARAMETER DETERMINATION BY ANALYSIS OF APPARENT SHAPE

A. Screen coordinates and Bardeen coordinates

We show that the parameters of the Kerr-Newman black hole can be determined from its apparent shape, along with a concrete method [29]. For this method to be used for future

shadow observations, we assume that r_o is sufficiently large. This means that we consider the apparent shape on the so-called Bardeen coordinates (b_x, b_y) for the observer at spatial infinity. Note that the apparent shape on the screen coordinates of the Kerr-Newman black hole for an observer at spatial infinity is a point. The Bardeen coordinates (b_x, b_y) is defined as follows:

$$b_x := \lim_{r \rightarrow \infty} \frac{-rk^{(\phi)}}{k^{(t)}} = (\ell + \ell_p) \csc i, \quad (49)$$

$$b_y := \lim_{r \rightarrow \infty} \frac{rk^{(\theta)}}{k^{(t)}} = (\mathbb{Q} + a^2 \cos^2 i - \ell \cot^2 i)^{1/2}, \quad (50)$$

where $(k^{(t)}, k^{(r)}, k^{(\theta)}, k^{(\phi)})$ are the tetrad components of the four-momentum of the massless test particle.

Although b_x contains a term for the conserved quantity ℓ_p of the principal null geodesic, this term is not present in the Bardeen coordinates for a zero-angular-momentum observer [32]. Since we are now assuming a Carter's observer, the origin of the Bardeen coordinates is shifted [37]. The analysis in this paper does not use information about the position on the Bardeen coordinates of the apparent shape. Therefore, the results of the analysis do not change for our assumed observer or for the case of the zero-angular-momentum observer.

Let us now describe the transformation from the screen coordinates to the Bardeen coordinates. In brief, Bardeen coordinates are the linearization of the screen coordinates of the distant observer [26, 37], as follows:

$$x = b_x r_o^{-1} + O(r_o^{-2}) \quad (r_o \rightarrow \infty), \quad (51)$$

$$y = b_y r_o^{-1} + O(r_o^{-2}) \quad (r_o \rightarrow \infty). \quad (52)$$

From here on in the following subsections in Sec. IV, the apparent shape on the Bardeen coordinates of the Kerr-Newman black hole will be the target of our analysis.

B. Uniqueness of apparent shape on the Bardeen coordinates

We prove the uniqueness of the apparent shape on the Bardeen coordinates of the Kerr-Newman black hole. Even if the apparent shape on the screen coordinates of a Kerr-Newman black hole is not unique, it does not necessarily mean that the apparent shape on the Bardeen coordinates of the Kerr-Newman black hole is non-unique.

The functions b_x and b_y^2 are rational functions with r_* as a variable. Note that the function is defined at $a_* \neq 0$. First, we analyze the rational function b_x . The condition under which the resultant for the numerator and denominator of the rational function b_x vanishes is as follows:

$$a_*^3 (a_*^2 + Q_*^2 - 1) \sin^3 i = 0. \quad (53)$$

The irreducible rational function b_x follows:

$$b_x = \begin{cases} \frac{\sum_{n=0}^3 s_n r_*^n}{\sum_{n=0}^1 t_n r_*^n} & (0 < a_*^2 + Q_*^2 < 1) \\ \frac{\sum_{n=0}^2 \bar{s}_n r_*^n}{\bar{t}_0} & (a_*^2 + Q_*^2 = 1) \end{cases}, \quad (54)$$

where

$$\begin{aligned} s_0 &= 2a_*^2 \cos^2 i, & s_1 &= 3a_*^2 + 4Q_*^2 - a_*^2 \cos 2i, & s_2 &= -6, & s_3 &= 2, \\ t_0 &= -2a_* \sin i, & t_1 &= 2a_* \sin i, \end{aligned}$$

and

$$\begin{aligned} \bar{s}_0 &= -2a_*^2 \cos^2 i, & \bar{s}_1 &= -4, & \bar{s}_2 &= -2, \\ \bar{t}_0 &= 2a_* \sin i. \end{aligned}$$

Next, the condition under which the resultant for the numerator and denominator of the rational function b_y^2 is zero is as follows:

$$a_*^{12} (a_*^2 + Q_*^2 - 1)^2 (a_*^2 \cos^2 i + Q_*^2 - 1)^2 \sin^{12} i = 0. \quad (55)$$

Then the irreducible rational function b_y^2 is as follows:

$$b_y^2 = \begin{cases} \frac{\sum_{n=0}^6 u_n r_*^n}{\sum_{n=0}^2 v_n r_*^n} & (0 < a_*^2 + Q_*^2 < 1) \\ \frac{\sum_{n=0}^4 \bar{u}_n r_*^n}{\bar{v}_0} & (a_*^2 + Q_*^2 = 1) \end{cases}, \quad (56)$$

where

$$\begin{aligned} u_0 &= -8a_*^4 \cos^4 i, & u_1 &= 8a_*^2 \cos^2 i (-3a_*^2 - 4Q_*^2 + a_*^2 \cos 2i), \\ u_2 &= -3a_*^4 - 32Q_*^4 + 8a_*^2 (3 - 4Q_*^2) - 4a_*^2 (-6 + a_*^2) \cos 2i - a_*^4 \cos 4i, \\ u_3 &= 32(a_*^2 + 3Q_*^2), & u_4 &= -8(9 + a_*^2 + 4Q_*^2 + a_*^2 \cos 2i), & u_5 &= 48, & u_6 &= -8, \\ v_0 &= 8a_*^2 \sin^2 i, & v_1 &= -16a_*^2 \sin^2 i, & v_2 &= 8a_*^2 \sin^2 i, \end{aligned}$$

and

$$\begin{aligned}\bar{u}_0 &= -8a_*^4 \cos^3 i \cot i, & \bar{u}_1 &= -32a_*^2 \cos i \cot i, & \bar{u}_2 &= -16(a_*^2 - 2) \csc i + 16a_*^2 \sin i, \\ \bar{u}_3 &= 32 \csc i, & \bar{u}_4 &= -8 \csc i, \\ \bar{v}_0 &= 8a_*^2 \sin i.\end{aligned}$$

Let us consider the case where $a_* \neq 0$.

For a nonextreme Kerr-Newman black hole, we assume that $b_x(r_*; a_*, Q_*, i) = b_x(r_*; a'_*, Q'_*, i')$. From the coefficient t_1 , we derive $a_* \sin i = a'_* \sin i'$. Analyzing the coefficient s_0 and s_1 , we conclude that $a_* = a'_*$ and $i = i'$. Additionally, we assume that $b_y^2(r_*; a_*, Q_*, i) = b_y^2(r_*; a'_*, Q'_*, i')$. From the coefficient u_3 , we deduce that $Q = Q'$.

Considering the case of an extreme Kerr-Newman black hole, we assume that $b_x(r_*; a_*, Q_*, i) = b_x(r_*; a'_*, Q'_*, i')$. From the coefficient \bar{t}_0 , we determine that $a_* \sin i = a'_* \sin i'$. Furthermore, we assume that $b_y^2(r_*; a_*, Q_*, i) = b_y^2(r_*; a'_*, Q'_*, i')$. By comparing \bar{u}_3 , we establish that $i = i'$, which implies $a_* = a'_*$. Assuming an extreme black hole, it follows that $Q = Q'$.

Now we consider the case where $a_* = 0$.

In this case, we examine the apparent shape of the Reissner-Nordström black hole. Since the Reissner-Nordström black hole is spherically symmetric, there is no rotation axis, and thus, the parameter i is not needed.

The apparent shape of the Reissner-Nordström black hole is a circle. The radius of the circle is a monotonically decreasing function with respect to the parameter Q_* [38]. This means that the apparent shape of the Reissner-Nordström black hole is unique.

Thus, the apparent shape of the Kerr-Newman black hole on the Bardeen coordinates is unique.

C. Map from parameter space to apparent-shape library

As we saw in the previous section, for a given parameters, an apparent shape can be determined. From this, we can consider a map from a parameter space to an apparent-shape library. The parameter space P is defined as

$$P := \left\{ (M, a, Q, i) \left| 0 \neq \frac{a}{M}, 0 \leq a^2 + Q^2 \leq M^2, 0 < i \leq \frac{\pi}{2} \right. \right\} \cup P_0, \quad (57)$$

where

$$P_0 := \left\{ (M, 0, Q, 0) \mid 0 \leq \frac{Q}{M} \leq 1 \right\}. \quad (58)$$

When the specific angular momentum a is zero, the black hole is spherically symmetric and has no axis of rotation. Hence, the inclination angle i need not be considered. The subset P_0 of P corresponds to the case where the black hole is a Reissner-Nordström black hole. The apparent-shape library S is defined as the set of all possible apparent shapes that can be generated by the system of the black hole, light source, and observer. The map f_1 from the parameter space P to the apparent-shape library S is defined as

$$f_1 : P \ni (M, a, Q, i) \mapsto \{(b_x(r_s), b_y(r_s)) \mid r_s \in I\} \in S. \quad (59)$$

The apparent shape is not explicitly dependent on mass M , but is determined by four dimensionless parameters (r_{o*}, a_*, Q_*, i) . Then, we define the equivalence relation \sim in parameter space P as follows:

$$(M, a, Q, i) \sim (M', a', Q', i') \stackrel{\text{def}}{\iff} \begin{cases} a/M = a'/M' \\ Q/M = Q'/M' \\ i = i' \end{cases}. \quad (60)$$

In Sec. IV, we see that the following map \tilde{f}_1 is injective:

$$\tilde{f}_1 : P/\sim \ni [(M, a, Q, i)] \mapsto f_1((M, a, Q, i)) \in S. \quad (61)$$

That is, each equivalence class $[(M, a, Q, i)]$ in quotient space P/\sim is mapped to one element in the apparent-shape library S . This is a paraphrase of the proposition that an apparent shape of Kerr-Newman black hole on Bardeen coordinates is unique.

D. Observables of apparent shape

We now obtain the observables of the apparent shape. An observable is defined as a quantity that represents a characteristic of the apparent shape and that can be derived from the apparent shape. The observables we need must be able to distinguish between all the apparent shapes in the apparent-shape library. We present observables with such properties along with the derivation process.

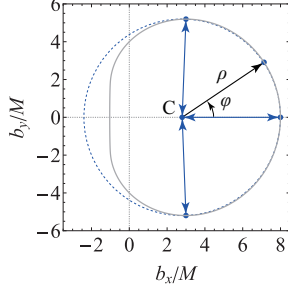


FIG. 4. Polar coordinates (ρ, φ) with origin at the center C of the apparent shape of the Kerr-Newman black hole.

The observables are derived independently of the position of the apparent shape in the screen coordinates. First, as shown in Fig. 4, we consider a circle passing through the top, bottom, and rightmost points of the apparent shape, and define the center of the circle as the center C of the apparent shape. The apparent shape can be shown in polar coordinates (ρ, φ) with the origin at the center C . We define a map f_2 from the apparent-shape library to the set of all simple closed curves G as follows:

$$f_2 : S \ni s \mapsto \{(\rho(\varphi) \cos \varphi, \rho(\varphi) \sin \varphi) \mid 0 \leq \varphi < 2\pi\} \in G. \quad (62)$$

The range of the map f_2 is denoted by $G_0 = f_2(S)$. We refer to an element of G_0 as a centered apparent shape.

We now consider the complex Fourier series representation of the function $\rho(\varphi)$:

$$\rho(\varphi) = \sum_{n=-\infty}^{\infty} c_n e^{in\varphi}, \quad (63)$$

$$c_n = \frac{1}{2\pi} \int_{-\pi}^{\pi} \rho(\varphi) e^{-in\varphi} d\varphi. \quad (64)$$

Since $\rho(\varphi)$ is a real function, $c_{-n} = c_n^*$ holds. As $\rho(\varphi)$ is piecewise smooth, its complex Fourier series converges to the function itself. Due to the symmetry of the apparent shape, expressed as $\rho(-\varphi) = -\rho(\varphi)$, the Fourier coefficients c_n are real.

In our analysis, we use up to the tenth Fourier coefficients. Let us define d as the map from a centered apparent shape to its eleven Fourier coefficients, denoted by $\mathbf{c} = (c_0, c_1, c_2, c_3, c_4, c_5, c_6, c_7, c_8, c_9, c_{10})$.

Principal component analysis is a method of finding new variables, called principal components, that maximize variance from multiple variables in a given data set [39]. In general, the map from multi-variables to principal components is an orthogonal transformation. To

facilitate the principal component analysis of the Fourier coefficients, we need to define the map f_3 as follows:

$$f_3 : G_0 \ni g \mapsto (d(g), C) \in C \times \{C\}, \quad (65)$$

where the Fourier coefficient space C is defined by $C := d(G_0)$. Principal component analysis is a method that is performed on data that holds a finite number of records. We sample 50^3 elements from the Fourier coefficient space C to create data C_s . To maintain the reproducibility of the results in the paper, we provide the sampled data C_s as Supplemental Material to the paper [40]. For the sampled data C_s , we perform a principal component analysis.

Principal components are obtained by orthogonal transforming each element of C . The transformation matrix of this orthogonal transformation is an eleventh order orthogonal matrix \mathbf{A} , which is obtained from the data C_s by the algorithm of principal component analysis [29, 39]. We also provide \mathbf{A} as Supplemental Material to the paper [41].

The principal component space Z is the set in which each element \mathbf{c} of the Fourier coefficient space C is orthogonally transformed by the transformation matrix \mathbf{A} . We define the map f_4 as follows:

$$f_4 : C \times \{C\} \ni (\mathbf{c}, C) \mapsto \mathbf{z} = (z_1, z_2, z_3, z_4, z_5, z_6, z_7, z_8, z_9, z_{10}, z_{11}) := \mathbf{c}\mathbf{A} \in Z. \quad (66)$$

In the algorithm of principal component analysis, the variance and covariance of the entire data is computed, thus C is explicitly indicated as the input to the map f_4 .

The entire set of elements consisting of the first three components of each element of the principal component space Z is defined as the observables space O . We define projection f_5 as follows:

$$f_5 : Z \ni \mathbf{z} \mapsto (z_1, z_2, z_3) \in O. \quad (67)$$

Finally, as shown in Fig. 5, we define the composite map f from the quotient space P/\sim to the observables space O as

$$f := f_5 \circ f_4 \circ f_3 \circ f_2 \circ \tilde{f}_1. \quad (68)$$

We refer to the first, second, and third components of (z_1, z_2, z_3) as the size, primary distortion, and secondary distortion, respectively. The isosurfaces of the observables are depicted

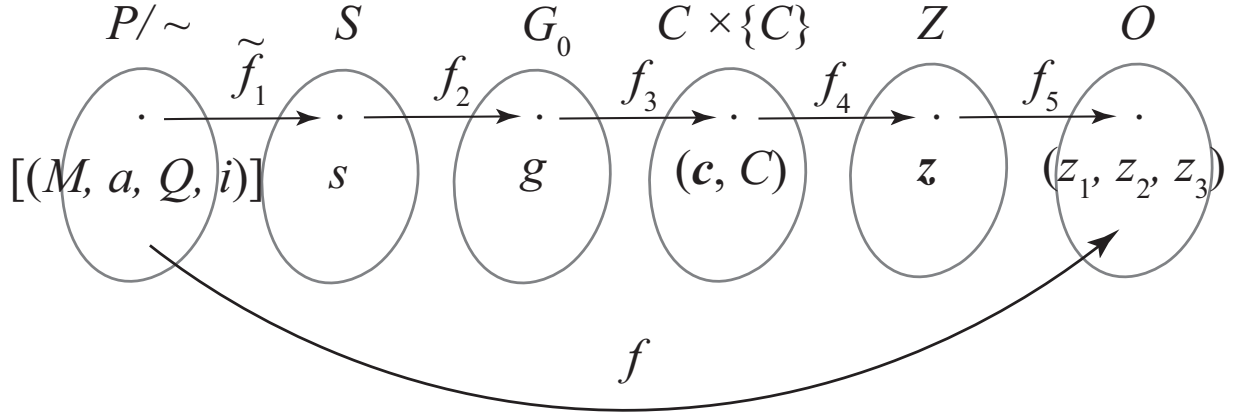


FIG. 5. Composite map f from the quotient parameter space P/\sim to the observable space O

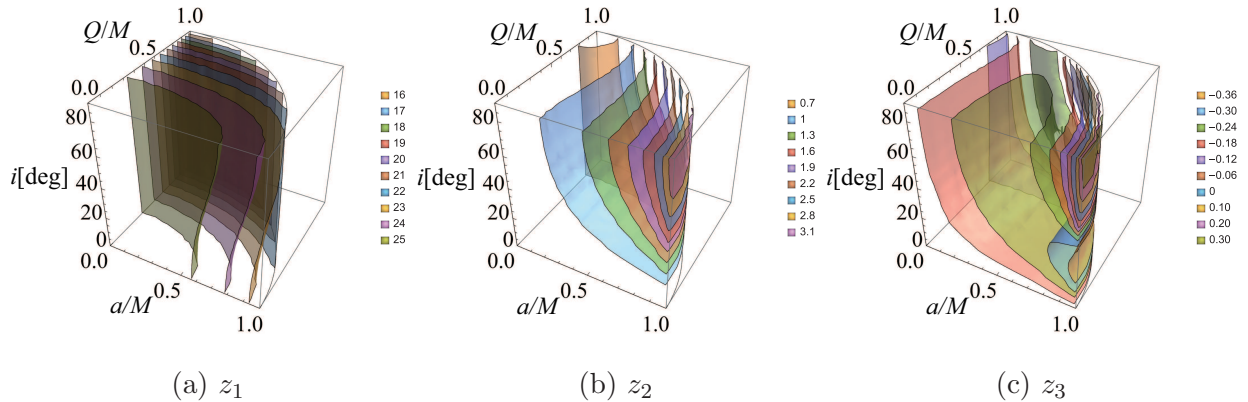


FIG. 6. (a) An isosurface map of the size z_1 . (b) An isosurface map of the primary distortion z_2 . (c) An isosurface map of the secondary distortion z_3 .

in Fig. 6. We have provided data on the parameters and their corresponding principal components in Supplemental Material. In the next subsection, we show that the map f from quotient parameter space P/\sim to observables space O is injection. We then conclude that the dimensionless parameters (a_*, Q_*, i) can be determined from the apparent shape.

E. Parameter determination

Figure 6(a) shows that the size of the apparent shape is almost independent of the inclination angle i . When the specific angular momentum is zero, the intersection of the isosurfaces with the Q_*-i plane is parallel to the i -axis. This is because when $a_* = 0$, the black hole has no axis of rotation and its apparent shape is a circle. Additionally, we can say that the larger the electric charge Q_* , the larger the size. As shown in Fig. 6(b), the

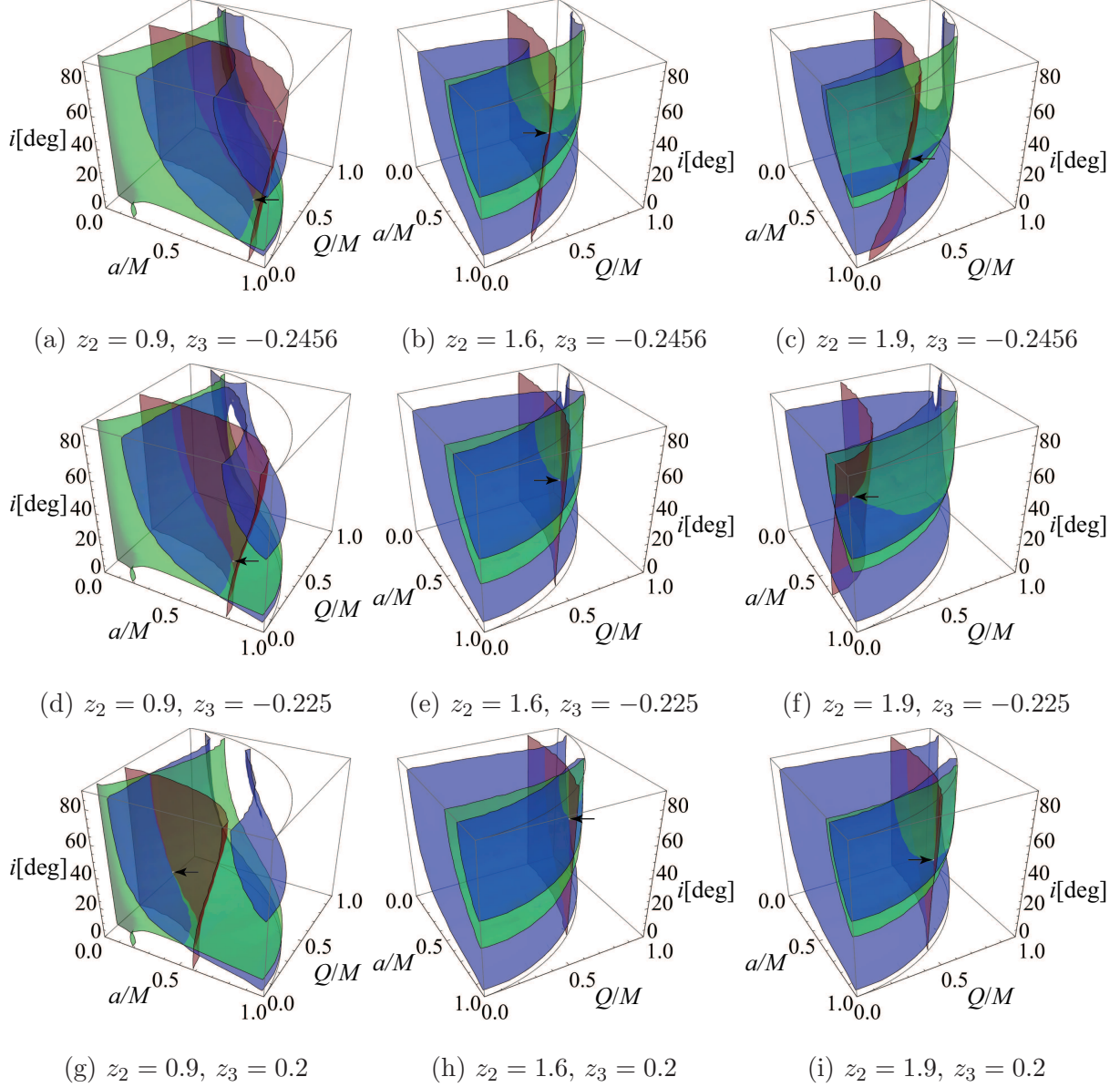


FIG. 7. The isosurfaces of the size z_1 (the red surfaces), the primary distortion z_2 (the green surfaces), and the secondary distortion z_3 (the blue surfaces). In (a), (b), (c), (d), (e), (f), (g), (h), and (i), sizes z_1 are 23.2, 22, 22.5, 24, 21, 24.5, 24.95, 20, and 21, respectively.

primary distortion is the deformation from the circle of the apparent shape, which differs between regions of small and large specific angular momentum a_* . The secondary distortion, depicted in Fig. 6(c), represents the common distortion effect between regions of small and large specific angular momentum a_* .

Varying the values of the three observables (z_1, z_2, z_3), the isosurfaces of the three observables are drawn in Fig. 7. As can be seen in Fig. 7, in all cases, the isosurfaces of the

three observables intersect at a single point. This indicates that the map f from P/\sim to O is injective. In other words, if the apparent shape of the black hole can be obtained by observation, the dimensionless parameters (a_*, Q_*, i) can be uniquely determined. Eventually, we can determine all four parameters (M, a, Q, i) if even one value of M , a or Q is known a priori from another observation.

F. Demonstration

Assuming that the shadow of a black hole is observed more accurately, we will demonstrate our method of determining parameters from the shadow of a black hole. Specifically, we assume that not only the radius of the shadow but also its distortion is accurately observed. Currently, only the radius of the black hole shadow is known for M87* [4].

First, one calculates the Fourier coefficients of the observed apparent shape up to the tenth order. Suppose that the Fourier coefficient \mathbf{c} has the value

$${}^t\mathbf{c} = \begin{pmatrix} -24.519 \\ -0.15890 \\ 1.1701 \\ 0.092009 \\ 1.0223 \\ 0.10407 \\ 1.0066 \\ 0.099632 \\ 0.98681 \\ 0.093727 \\ 0.96167 \end{pmatrix}. \quad (69)$$

Then, using the transformation matrix \mathbf{A} of Supplemental Material of the paper [41], one

finds the principal components \mathbf{z} from the Fourier coefficients \mathbf{c} .

$${}^t\mathbf{z} = {}^t\mathbf{A}{}^t\mathbf{c} = \begin{pmatrix} 24.602 \\ 1.1103 \\ -0.27511 \\ -0.037610 \\ 0.0082606 \\ 0.0017246 \\ 0.00021964 \\ -0.00015774 \\ 0.000070632 \\ 0.000011432 \\ 0.0000030476 \end{pmatrix}. \quad (70)$$

Note that the first three components of \mathbf{z} are the values of the observables z_1 , z_2 , and z_3 . From the data provided as Supplemental Material [40], we can immediately draw the isosurfaces of the three observables at these values in (a_*, Q_*, i) space. Then, by identifying the point where the isosurfaces intersect, we can find the values of the dimensionless parameters (a_*, Q_*, i) corresponding to the observables. Thus eventually, the values of the dimensionless parameters (a_*, Q_*, i) are determined as follows:

$$(a_*, Q_*, i) = (0.70991, 0.011152, 31.500). \quad (71)$$

If any one of mass M , specific angular momentum a , or electric charge Q is known a priori from another observation, the four parameters (M, a, Q, i) can be determined.

V. CONCLUSION

We have analyzed the apparent shape of Kerr-Newman black holes without accretion disks, i.e., bare Kerr-Newman black holes. Our investigation focused on determining dimensionless parameters from the apparent shape, considering cases where the observer is positioned at either a finite distance or spatial infinity. The dimensionless parameters of the system, comprising the black hole, light source, and observer, are the dimensionless specific angular momentum a_* , the dimensionless electric charge Q_* , the inclination angle i , and the dimensionless distance r_{o*} .

We analytically proved that the apparent shape of a Kerr-Newman black hole in Bardeen coordinates is unique. A crucial point in this proof was that the equation governing the apparent shape is an irreducible rational function. This uniqueness, in principle, implies that the dimensionless parameters (a_*, Q_*, i) of the Kerr-Newman black hole can be determined from its apparent shape.

Additionally, we demonstrated that these dimensionless parameters (a_*, Q_*, i) can be extracted from the apparent shape in Bardeen coordinates using our proposed method. The key to this method is that the three principal components (z_1, z_2, z_3) of the eleven Fourier coefficients of the apparent shape in Bardeen coordinates correspond one-to-one with the three dimensionless parameters (a_*, Q_*, i) . Our approach could be applied in the future to determine parameters for various black hole solutions based on the apparent shape, particularly when both the size and distortion of the black hole shadow are observable.

Interestingly, we also analytically showed that the apparent shape of a Kerr-Newman black hole at a finite distance is not unique. For instance, the apparent shape of a Kerr-Newman black hole with zero specific angular momentum is a circle. Although both the distance r_{o*} and the electric charge Q_* influence the radius of this circle, it was found that these two parameters cannot be independently determined from the radius, even if the apparent shape is observed.

The uniqueness of the apparent shapes in Bardeen coordinates, contrasted with the non-uniqueness in screen coordinates, reveals an aspect of the structure of the image library.

In this paper, we simplified our model by assuming a black hole without an accretion disk. The next step will involve analyzing a more realistic black hole model that includes an accretion disk. In that case, the uniqueness of the apparent shape of the black hole at finite distance may hold. Our results strengthen the direction of research in black hole shadow observation.

ACKNOWLEDGEMENTS

This work was supported in part by JSPS KAKENHI Grant No. JP22K03623 (U.M.).

- [1] K. Akiyama *et al.* [Event Horizon Telescope], *Astrophys. J. Lett.* **875**, L1 (2019)
doi:10.3847/2041-8213/ab0ec7 [arXiv:1906.11238 [astro-ph.GA]].
- [2] K. Akiyama *et al.* [Event Horizon Telescope], *Astrophys. J. Lett.* **875**, no.1, L2 (2019)
doi:10.3847/2041-8213/ab0c96 [arXiv:1906.11239 [astro-ph.IM]].
- [3] K. Akiyama *et al.* [Event Horizon Telescope], *Astrophys. J. Lett.* **875**, no.1, L3 (2019)
doi:10.3847/2041-8213/ab0c57 [arXiv:1906.11240 [astro-ph.GA]].
- [4] K. Akiyama *et al.* [Event Horizon Telescope], *Astrophys. J. Lett.* **875**, no.1, L4 (2019)
doi:10.3847/2041-8213/ab0e85 [arXiv:1906.11241 [astro-ph.GA]].
- [5] K. Akiyama *et al.* [Event Horizon Telescope], *Astrophys. J. Lett.* **875**, no.1, L6 (2019)
doi:10.3847/2041-8213/ab1141 [arXiv:1906.11243 [astro-ph.GA]].
- [6] K. Akiyama *et al.* [Event Horizon Telescope], *Astrophys. J. Lett.* **910**, no.1, L12 (2021)
doi:10.3847/2041-8213/abe71d [arXiv:2105.01169 [astro-ph.HE]].
- [7] K. Akiyama *et al.* [Event Horizon Telescope], *Astrophys. J. Lett.* **910**, no.1, L13 (2021)
doi:10.3847/2041-8213/abe4de [arXiv:2105.01173 [astro-ph.HE]].
- [8] K. Akiyama *et al.* [Event Horizon Telescope], *Astrophys. J. Lett.* **930**, no.2, L12 (2022)
doi:10.3847/2041-8213/ac6674.
- [9] K. Akiyama *et al.* [Event Horizon Telescope], *Astrophys. J. Lett.* **930**, no.2, L13 (2022)
doi:10.3847/2041-8213/ac6675.
- [10] K. Akiyama *et al.* [Event Horizon Telescope], *Astrophys. J. Lett.* **930**, no.2, L14 (2022)
doi:10.3847/2041-8213/ac6429.
- [11] K. Akiyama *et al.* [Event Horizon Telescope], *Astrophys. J. Lett.* **930**, no.2, L15 (2022)
doi:10.3847/2041-8213/ac6736.
- [12] K. Akiyama *et al.* [Event Horizon Telescope], *Astrophys. J. Lett.* **930**, no.2, L16 (2022)
doi:10.3847/2041-8213/ac6672.
- [13] K. Akiyama *et al.* [Event Horizon Telescope], *Astrophys. J. Lett.* **930**, no.2, L17 (2022)
doi:10.3847/2041-8213/ac6756.

- [14] C. Darwin, in “The gravity field of a particle,” Proceedings of the Royal Society of London. Series A.249, no.1257 (Jan., 1959) 180-194.
- [15] J. M. Bardeen, in “Black Holes,” ed. C. DeWitt and B. DeWitt, New York, Gordon & Breach (1973).
- [16] A. de Vries, *Class. Quant. Grav.* **17**, no.1, 123-144 (1999) doi:10.1088/0264-9381/17/1/309
- [17] K. Hioki and U. Miyamoto, *Phys. Rev. D* **78**, 044007 (2008), [arXiv:0805.3146 [gr-qc]].
- [18] C. Bambi and N. Yoshida, *Class. Quant. Grav.* **27**, 205006 (2010) doi:10.1088/0264-9381/27/20/205006 [arXiv:1004.3149 [gr-qc]].
- [19] L. Amarilla, E. F. Eiroa and G. Giribet, *Phys. Rev. D* **81**, 124045 (2010) doi:10.1103/PhysRevD.81.124045 [arXiv:1005.0607 [gr-qc]].
- [20] L. Amarilla and E. F. Eiroa, *Phys. Rev. D* **87**, no.4, 044057 (2013) doi:10.1103/PhysRevD.87.044057 [arXiv:1301.0532 [gr-qc]].
- [21] S. W. Wei and Y. X. Liu, *JCAP* **11**, 063 (2013) doi:10.1088/1475-7516/2013/11/063 [arXiv:1311.4251 [gr-qc]].
- [22] U. Papnoi, F. Atamurotov, S. G. Ghosh and B. Ahmedov, *Phys. Rev. D* **90**, no.2, 024073 (2014) doi:10.1103/PhysRevD.90.024073 [arXiv:1407.0834 [gr-qc]].
- [23] S. W. Wei, P. Cheng, Y. Zhong and X. N. Zhou, *JCAP* **08**, 004 (2015) doi:10.1088/1475-7516/2015/08/004 [arXiv:1501.06298 [gr-qc]].
- [24] B. P. Singh and S. G. Ghosh, *Annals Phys.* **395**, 127-137 (2018) doi:10.1016/j.aop.2018.05.010 [arXiv:1707.07125 [gr-qc]].
- [25] Z. Stuchlík and J. Schee, *Eur. Phys. J. C* **79**, no.1, 44 (2019) doi:10.1140/epjc/s10052-019-6543-8.
- [26] N. Tsukamoto and R. Kase, [arXiv:2404.06414 [gr-qc]].
- [27] K. Hioki and K. i. Maeda, *Phys. Rev. D* **80**, 024042 (2009) doi:10.1103/PhysRevD.80.024042 [arXiv:0904.3575 [astro-ph.HE]].
- [28] K. Hioki and U. Miyamoto, *Phys. Rev. D* **107**, no.4, 044042 (2023) doi:10.1103/PhysRevD.107.044042 [arXiv:2210.02164 [gr-qc]].
- [29] K. Hioki and U. Miyamoto, *Phys. Rev. D* **109**, no.4, 044030 (2024) doi:10.1103/PhysRevD.109.044030 [arXiv:2311.16802 [gr-qc]].
- [30] E. T. Newman, R. Couch, K. Chinnapared, A. Exton, A. Prakash and R. Torrence, *J. Math. Phys.* **6**, 918-919 (1965) doi:10.1063/1.1704351

- [31] S. Chandrasekhar, “The mathematical theory of black holes”, Oxford Univ. Press (1992).
- [32] P. Kocherlakota *et al.* [Event Horizon Telescope], Phys. Rev. D **103**, no.10, 104047 (2021) doi:10.1103/PhysRevD.103.104047 [arXiv:2105.09343 [gr-qc]].
- [33] S. Vagnozzi, R. Roy, Y. D. Tsai, L. Visinelli, M. Afrin, A. Allahyari, P. Bambhaniya, D. Dey, S. G. Ghosh and P. S. Joshi, *et al.* Class. Quant. Grav. **40**, no.16, 165007 (2023) doi:10.1088/1361-6382/acd97b [arXiv:2205.07787 [gr-qc]].
- [34] A. Grenzebach, V. Perlick and C. Lämmerzahl, Phys. Rev. D **89**, no.12, 124004 (2014) doi:10.1103/PhysRevD.89.124004 [arXiv:1403.5234 [gr-qc]].
- [35] Z. Chang and Q. H. Zhu, Phys. Rev. D **102**, no.4, 044012 (2020) doi:10.1103/PhysRevD.102.044012 [arXiv:2006.00685 [gr-qc]].
- [36] D. Cox, J. Little and D. O’shea, “Using algebraic geometry”, Springer Science & Business Media (2005).
- [37] V. Perlick and O. Y. Tsupko, Phys. Rept. **947**, 1-39 (2022) doi:10.1016/j.physrep.2021.10.004 [arXiv:2105.07101 [gr-qc]].
- [38] A. F. Zakharov, F. De Paolis, G. Ingrosso and A. A. Nucita, Astron. Astrophys. **442**, no.3, 795-799 doi:10.1051/0004-6361:20053432 [arXiv:astro-ph/0505286 [astro-ph]].
- [39] Jolliffe, Ian T and Cadima, Jorge, “Principal component analysis: a review and recent developments,” Phil. Trans. R. Soc. A. **374**, 20150202 (2016).
- [40] See the Supplemental Material for table data on the dimensionless parameters, their corresponding Fourier coefficients, and principal components.
- [41] See the Supplemental Material for table data on the transformation matrix **A**.